HHS Public Access
Author manuscript
ACS Catal. Author manuscript; available in PMC 2019 February 02.

Published in final edited form as:
ACS Catal. 2018 February 2; 8(2): 1448–1455. doi:10.1021/acscatal.7b03068.

Fe-mediated HER vs N_2RR: Exploring Factors that Contribute to Selectivity in $P_3^EFe(N_2)$ (E = B, Si, C) Catalyst Model Systems

Benjamin D. Matson and **Jonas C. Peters***
Division of Chemistry and Chemical Engineering, California Institute of Technology (Caltech), Pasadena, California 91125, United States

Abstract

Mitigation of the hydrogen evolution reaction (HER) is a key challenge in selective small molecule reduction catalysis. This is especially true of catalytic nitrogen (N_2) and carbon dioxide (CO_2) reduction reactions (N_2RR and CO_2RR, respectively) using H^+/e^- currency. Here we explore, via DFT calculations, three iron model systems, P_3^EFe (E = B, Si, C), known to mediate both N_2RR and HER, but with different selectivity depending on the identity of the auxiliary ligand. It is suggested that the respective efficiencies of these systems for N_2RR trend with the predicted N–H bonds strengths of two putative hydrazido intermediates of the proposed catalytic cycle, $P_3^EFe(NNH_2)^+$ and $P_3^EFe(NNH_2)$. Further, a mechanism is presented for undesired HER consistent with DFT studies, and previously reported experimental data, for these systems; bimolecular proton-coupled-electron-transfer (PCET) from intermediates with weak N–H bonds is posited as an important source of H_2, instead of more traditional scenarios that proceed via metal hydride intermediates and proton transfer/electron transfer (PT/ET) pathways. Wiberg bond indices provide additional insight into key factors related to the degree of stabilization of $P_3^EFe(NNH_2)$ species, factors that trend with overall product selectivity.

Keywords

nitrogen fixation; N_2RR; HER; hydrogen evolution; PCET; HAT; nitrogenase

Introduction

The reduction of nitrogen (N_2) to ammonia (NH_3) by nitrogenase enzymes (the nitrogen reduction reaction: N_2RR) has garnered substantial interest in the synthetic inorganic community for several decades. [1] In particular, the structural characterization of the FeMo-cofactor active site of biological nitrogen fixation, [2] and mechanistic uncertainties associated with this process, [3] have motivated studies of synthetic (primarily Mo and Fe) model systems that mediate N_2RR in the presence of proton and electron equivalents in organic solvent.[4-6] The mechanisms of these systems are at various stages of understanding.

*Corresponding Author jpeters@caltech.edu.

ASSOCIATED CONTENT
Supporting Information.
The Supporting Information is available free of charge on the ACS Publications website.
Complete computational details, molecular geometries from the computations, additional computations and analysis (PDF)

Experimental[4, 5 , 6] and theoretical (predominantly Mo)[7] studies have been undertaken to provide insight.

Single-site iron model complexes, such as $P_3^BFe(N_2)^-$ and $P_3^BFe^+$ (Figure 1), catalyze N_2RR under a variety of conditions and driving forces, with reported selectivities (to date) for NH_3 generation as high as 72% based on reductant consumed.[4e] In addition, conditions have been reported under which $P_3^CFe(N_2)^-$ and $P_3^{Si}Fe(N_2)^-$ also catalyze N_2RR to varying degrees, with the $P_3^{Si}Fe$-system being far more efficient at the hydrogen evolution reaction (HER) than N_2RR compared to P_3^BFe and P_3^CFe.[4d,8] We are naturally interested in understanding the mechanism/s by which catalysis in these respective systems occurs, and in exploring alternative systems that might function similarly. Of interest to the present study is the interplay between efficiency for the N_2RR and HER on the P_3^BFe scaffold and its isostructural congeners $P_3^{Si}Fe$ and P_3^CFe. In particular, can we elucidate some of the salient factors that dictate overall product selectivity for NH_3 versus H_2 in these respective systems?

Herein we use DFT calculations to explore this question. We examine the comparative feasibility of HER via proton-coupled electron transfer (PCET) [9] from several putative $Fe(N_xH_y)$ early intermediates, using electronic structure calculations coupled with predicted N–H bond strengths, thermodynamic driving forces, and electron-transfer (ET) kinetics as mechanistic probes. Acknowledging the likelihood that numerous and potentially competing factors may be at play, the formation, electronic structure, and reactivity of a key common intermediate, $Fe(NNH_2)^+$, is highlighted to be an important factor in the divergent selectivity profile of P_3^BFe (and P_3^CFe) relative to the $P_3^{Si}Fe$ system.

Computational Methods

All calculations were performed using dispersion corrected density functional theory (DFT-D_3) using Grimmes dispersion correction. [10] All calculations were done using the full P_3^EFe scaffold with the TPSS functional[11] and a def2-TZVP basis set on transition metals and a def2-SVP basis set on all other atoms.[12]

All stationary point geometries were optimized using NWChem 6.3[13] or Orca 3.0.3.[14] To ensure consistency in grid size, all reported single point and thermodynamic energies were performed using Orca 3.0.3. Frequency calculations were used to confirm the presence of true minima and to obtain gas phase free-energy values at 195 K (G_{gas}). Solvation corrections were performed using the COSMO-SMD continuum model. [15] The solvation free energy was approximated using gas phase and solvated single point energies ($\Delta G_{solv} \approx E_{soln} - E_{gas}$). Finally, the free-energy of the solvated species at 195 K was calculated using the gas-phase free-energy and the solvation free-energy ($G_{soln,195K} = G_{gas,195k} + \Delta G_{solv}$).[16]

The accuracy of the described computational methodology was measured by comparison to several experimental benchmarks of interest. In addition to ensuring good agreement between computed and crystallographically determined structural data, experimentally determined bond dissociation enthalpies ($BDFE_{N-H}$) of the compounds $P_3^{Si}Fe(CNH)^+$, $P_3^{Si}Fe(CNH)$, $P_3^{Si}Fe(CNMeH)^+$, $P_3^{Si}Fe(CNMeH)$ and $P_3^{Si}Fe(NNMeH)^+$ could be faithfully reproduced within ±2 kcal/mol (See SI for full description).[4h] As a further point of

calibration, the calculated singlet-triplet energy gap and the redox potentials of $P_3^BFe(NNMe_2)$ and $P_3^{Si}Fe(NNMe_2)^+$ are in good agreement with the experimentally determined values (within ±1.5 kcal/mol, and ±3 kcal/mol (±130 mV vs $Fc^{+/0}$), respectively ; see SI).[4g,4,17]

Reduction kinetics were calculated using the standard Marcus equation relating activation barrier with driving force and total reorganization energy ($\lambda_{tot} = \lambda_{is} + \lambda_{os}$).[18] The inner-sphere reorganization energy for electron transfer ($\lambda_{is,ET}$) was estimated assuming non-adiabatic behavior and by calculating the difference between the single point energies of the relevant species in its ground state and the corresponding single point energy of this ground state in the oxidized or reduced geometry (Eq. 1).

$$\lambda_{is,ET} = \left[E\left(Fe^{ox}{}_{ox}\right) - E\left(Fe^{ox}{}_{red}\right)\right] + \left[E\left(Fe^{red}{}_{red}\right) - E\left(Fe^{red}{}_{ox}\right)\right]$$

The outer-sphere reorganization energy was calculated by assuming a barrier of 1.0 kcal/mol for the reduction of $P_3^BFe(NNH_2)^+$ followed by calculation of λ_{tot} using this barrier and λ_{is}, as calculated by Eq. 1. A continuum solvation model was used to confirm that $\lambda_{os} \approx \lambda_{is}$ (See SI for full description).[18] Reduction barriers for $P_3^{C/Si}Fe(NNH_2)^+$ were subsequently calculated relative to $P_3^BFe(NNH_2)^+$.

Results and Discussion

To set the stage for the present study, previously reported catalytic N_2-to-NH_3 conversion studies by P_3^EFe (E = B, C, and Si) under an atmosphere of N_2 at −78 °C in Et_2O, using KC_8 and $[(Et_2O)_2H][BAr^F{}_4]$ ($HBAr^F{}_4$, $BAr^F{}_4$ = tetrakis-(3,5-bis(trifluoromethyl)phenyl)borate) as the reductant and acid source,[4a,d] established P_3^BFe as the most efficient catalyst for N_2RR; the highest reported efficiency for this system (under these conditions) was 45 ± 3% (48 equiv acid; 58 equiv reductant). For comparison, the $P_3^{Si}Fe$ system provided a conversion efficiency of only 5 ± 3%. The P_3^CFe catalyst system was reasonably active at 36 ± 6% (note: ~25% lower substrate loading was used for this P_3^CFe value[4d]). Measurement of HER activity established $P_3^{Si}Fe(N_2)^-$ (88% per added acid equiv) as a significantly more efficient HER catalyst than $P_3^BFe(N_2)^-$ (40% per added acid equiv) under analogous conditions.[4d] N_2RR catalysis by P_3^EFe (E = B, Si) has also been studied in the presence of milder reagents (e.g., $Cp^*{}_2Co$ and $[H_2NPh_2][OTf]$ or $[H_3NPh][OTf]$); under these conditions only the P_3^BFe system is catalytically active.

Previous studies of the P_3^BFe and $P_3^{Si}Fe$ systems have also explored the generation and characterization of early stage intermediates of the N_2RR catalysis.[4e,f,g] Most salient, low temperature protonation of $P_3^EFe(N_2)^-$ (E = B, Si) with excess $HBAr^F{}_4$ affords the doubly protonated $P_3^EFe(NNH_2)^+$ species (Figure 2).[4f,g] As expected, corresponding DFT calculations (this work) are consistent with thermodynamically favored formation of $P_3^EFe(NNH)$ via proton transfer (Figure 2); another favorable proton transfer forms $P_3^EFe(NNH_2)^+$.

DFT Support for Slow Fe Protonation and Fast Fe-N_xH_y Formation

Although metal hydride (M–H) species are most typically invoked as intermediates of transition-metal catalyzed HER,[19] we do not think Fe–H species are the primary players in H_2 formation by the present systems. Several experimental observations are consistent with this idea. Foremost among them is that low temperature addition of stoichiometric acid (e.g., $HBAr^F_4$) to any of the anions, $P_3^EFe(N_2)^-$, causes overall oxidation to their corresponding neutral products, $P_3^EFe(N_2)$, along with release of 0.5 equiv H_2.[4a,d] This is noteworthy because for E = Si or C the diamagnetic hydride products, $P_3^EFe(N_2)(H)$, are very stable species and are formed during catalysis as end products.[4b,d] We posit that reactive $P_3^EFe(N_xH_y)$ intermediates instead undergo net bimolecular HAT reactions to liberate H_2 via N_xH_y-ligand-mediated steps (*vida infra*). While iron hydrides (Fe–H) can tie up the population of active catalyst, in our view they are unlikely to be intermediates of the dominant HER pathway.

To speak to this hypothesis computationally, we focus on one acid source, $HBAr^F_4$, as it has been the subject of the most extensive comparative study.[4d] The solid-state empirical formula of $HBAr^F_4$ reveals the presence of two ethers per $HBAr^F_4$ ($[(Et_2O)_2H][BAr^F_4]$) [20] To determine the preferred solution-state structure of this acid, optimizations were performed in which a Et_2OH^+ species was provided with 0, 1 or 2 explicit Et_2O molecules with which to hydrogen bond. We found that $[(Et_2O)_2H]^+$ speciation was lowest in free-energy, with $[(Et_2O)_3H]^+$ and $[Et_2OH]^+$ higher in energy by +7.0 and +8.2 kcal/mol, respectively (see SI).

The structure of $HBAr^F_4$ is particularly crucial for Fe protonation, as a pre-equilibrium formation of the $[Et_2OH]^+$ appears to be required, as evidenced by relaxed surface scans. The need for dissociation of Et_2O prior to Fe protonation provides a lower bound on the barrier of +8.2 kcal/mol. The requirement of $[Et_2OH]^+$ as the active acid, as opposed to $[(Et_2O)_2H]^+$, is presumably steric in origin and may speak, in part, to the importance of bulky isopropyl-phosphino substituents in these catalysts. Our lab recently reported that a structurally related $P_3^{Si}Os(N_2)^-$ complex is an active catalyst for N_2RR. [21] In contrast to the $P_3^EFe(N_2)^-$ catalysts, stoichiometric $HBAr^F_4$ addition can protonate at the metal, generating Os-H species that are not catalytically active for N_2RR. Steric access to the larger Os center is presumably less restricted than it is for Fe.

The steric profile of the $Fe(N_2)$ unit suggests that functionalization of the β–N should not be subject to the same pre-equilibrium. This is consistent with relaxed surface scans, which show that the N_2 unit can be protonated in a concerted, low energy step in which an Et_2O molecule is favorably displaced by the nucleophilic β N-atom. Subsequent proton transfers yield Fe(NNH) with a low overall kinetic barrier (0.5–1.0 kcal/mol; see SI).

Fe–H formation is thermodynamically favored for all three scaffolds. We therefore presume that the dominant source of HER for these systems is not via Fe–H formation, but that hydride species are formed over the course of catalysis as thermodynamic products. We presume that both HER and N_2RR, under the conditions explored in this work, are operating

under kinetic control. In subsequent results and discussion, thermodynamics are assumed to be relevant within the context of kinetic parameters.

In addition to restricting our analysis to a single acid, $HBAr^F_4$, we focus on KC_8 as a reductant for several reasons. Most salient is that KC_8 is the only reductant that has been shown to produce catalytic yields of NH_3 for all scaffolds considered. This observation is attributed to the requirement of $Fe(N_2)^-$ formation during catalysis. While $P_3{}^BFe(N_2)^-$ can be formed with weaker reductants, namely $p^*{}_2Co$, the more reducing $P_3{}^{Si/C}Fe(N_2)^-$ is believed to be inaccessible under these conditions. Additionally, it has been noted that, when using KC_8 and $HBAr^F_4$, HER and N_2RR proceed with similar initial rates on $P_3{}^{Si}Fe$ and $P_3{}^BFe$ scaffolds,[4d] possibly due to $Fe(N_2)$ reduction being a common rate limiting step. Further the initial rates of N_2RR are similar between the scaffolds, which makes this reductant/acid combination well suited for a comparative study.

Despite the need to restrict the scope of this study to a specific catalysis cocktail, many of the conclusions should extend to other conditions reported for N_2RR catalysis using $P_3{}^EFe$ (and related) complexes. In particular, the $BDFE_{N\text{-}H}$ values reported herein are acid and reductant independent and hence provide insight into the anticipated stability and reactivity profiles of key early intermediates of N_2RR.

Calculation of $BDFE_{N\text{-}H}$ Values for Fe–N_xH_y Intermediates

Early stage intermediates of the type Fe(NNH) and $Fe(NNH_2)$ are expected to be highly reactive;[4e,h] thermochemical calculations reveal the presence of extremely weak N–H bonds in these systems, as shown by their calculated bond dissociation enthalpies ($BDFE_{N–H}$; Figure 3). In particular, as yet unobservable $P_3{}^EFe(NNH)$ intermediates are predicted to have extremely weak N–H bonds (< 40 kcal/mol), and should therefore be subject to rapid bimolecular loss of H_2 and generation of $P_3{}^EFe(N_2)$. By contrast, the $BDFE_{N\text{-}H}$ values of candidate $P_3{}^EFe(N_xH_y)$ intermediates that are further downstream (e.g., $Fe(N_2H_4)$, Fe(NH), $Fe(NH_2)$) are predicted to be significantly larger (Figure 3). This notion is consistent with the solution stability of characterized examples of such downstream intermediates, contrasting the high degree of solution instability of earlier intermediates.

Of particular interest herein is that the $BDFE_{N–H}$ values for the $P_3{}^{Si}Fe(NNH_2)^{n+}$ (n = 0, 1) system are lower than those for $P_3{}^{B/C}$, for a given overall charge. As discussed later, these different $BDFE_{N–H}$ values are rooted in the different valence electron counts, and hence electronic structures, of the respective $P_3{}^EFe$-systems.

For additional context, it is useful to consider reported $BDFE_{N–H}$ data for a related $P_3{}^{Si}Fe(CN)$-system. The relevant $P_3{}^{Si}Fe(CNH)$ species, isoelectronic with $P_3{}^BFe(NNH)$, is calculated to have a weak $BDFE_{N–H}$ of 43.5 kcal/mol, in close agreement to that of 41.4 kcal/mol determined experimentally.[4h] Accordingly, $P_3{}^{Si}Fe(CNH)$ loses 0.5 equiv H_2 rapidly in solution to afford $P_3{}^{Si}Fe(CN)$. In contrast, its oxidized cation, $P_3{}^{Si}Fe(CNH)^+$, has a much higher $BDFE_{N–H}$ (61.8 kcal/mol (calc); 61.9 kcal/mol (exp)); this species is stable to H_2 loss in solution and can be isolated and structurally characterized.

Considering these collected data and observations, and additional data discussed below, we presume that the earliest N_2RR intermediates in P_3^EFe-systems are very important for determining N_2RR versus HER selectivity; they engage in bimolecular H_2-evolving reactions that compete with productive N_2RR. We next consider aspects of the H–H bond-forming steps in these early P_3^EFe(N_xH_y) intermediates in more detail.

P_3^EFe(NNH) species are plausible candidates to consider with respect to selectivity since bimolecular H_2-evolving reactions can presumably result from their extremely weak N–H bonds (Figure 3; 31-17 kcal/mol). P_3^{Si}Fe(NNH), with a $BDFE_{N–H}$ estimated to be 8.2 kcal/mol lower than for P_3^BFe(NNH), might be reasonably expected to liberate H_2 more readily, thereby attenuating its N_2RR efficiency. However, the $BDFE_{N–H}$ for P_3^CFe(NNH) is calculated to be even lower (17.3 kcal/mol) than for P_3^{Si}Fe(NNH) (23 kcal/mol), despite the fact that P_3^CFe$(N_2)^-$ is appreciably more efficient for N_2RR. Hence, a trend is not evident on the basis of the Fe(NNH) intermediates, at least as related to their relative $BDFE_{N–H}$ values. Fe(NNH) intermediates are readily protonated to form Fe$(NNH_2)^+$ species in solution at low temperature (Figure 2). This likewise suggests that Fe(NNH) intermediates are unlikely to be primarily responsible for HER under catalytic conditions when a large excess of acid is present.[4f,g]

P_3^EFe(NNH_2) $BDFE_{N–H}$ values provide a more tractable trend: the respective calculated values are 38.2 kcal/mol for P_3^BFe, 34.4 kcal/mol for P_3^CFe, and 22.9 kcal/mol for P_3^{Si}Fe; the P_3^EFe–NNH_2 species that exhibits the most efficient N_2RR activity exhibits the strongest N-H bond, and the least efficient exhibits the weakest (Figure 3).

Calculated Reduction Kinetics of P_3^EFe$(NNH_2)^+$

To gain further insight into the respective role P_3^EFe$(NNH_2)^{+/0}$ (E = B, Si, C) species might play in dictating product selectivity, P_3^EFe$(NNH_2)^+$ reduction kinetics were derived using the standard Marcus equation relating the driving force and total reorganization energy with the ET activation barrier.[18] Comparison of the optimized Fe(NNH_2) and Fe$(NNH_2)^+$ redox pairs reveals significant differences in their respective reduction potentials and inner-sphere reorganization energies ($\lambda_{is,ET}$).

The P_3^BFe$(NNH_2)^+$ species is predicted to have a considerably more positive reduction potential (−1.2 V vs Fc/Fc^+) than P_3^{Si}Fe$(NNH_2)^+$ (−1.9 V; Table 1), resulting from their different valence electronic counts and electronic structures (see below). Given their dramatic difference in reduction potentials, the barrier for reduction (G*) is expected to sharply increase in moving from B to Si. Relative reduction barrier calculations, assuming G* = 1.0 kcal/mol for the reduction of P_3^BFe$(NNH_2)^+$, predict activation barriers that are 4–5 times higher in energy for the reduction of $P_3^{C/Si}$Fe$(NNH_2)^+$ versus P_3^BFe$(NNH_2)^+$ (Table 1). While the reduction of all three species should be more than readily accomplished by the strong reductant KC_8, $P_3^{C/Si}$Fe$(NNH_2)^+$ species are predicted to be significantly longer lived than the P_3^BFe$(NNH_2)^+$ congener.

To roughly quantify the differences in reduction rate between P_3^EFe$(NNH_2)^+$ species, and hence get a sense of their relative expected lifetimes, we turned to transition state theory. By

assuming a pre-exponential factor invariant across both scaffolds, reduction rates for $P_3^{Si}Fe(NNH_2)^+$ and $P_3^{C}Fe(NNH_2)^+$, normalized to $P_3^{B}Fe(NNH_2)^+$ (k_{rel}), were calculated ($k_{rel} = 2\times10^{-4}$ and 2×10^{-5}, respectively). Accordingly, we expect $P_3^{Si}Fe(NNH_2)^+$ and $P_3^{C}Fe(NNH_2)^+$ to be ~ 10^4 times longer-lived, respectively, than $P_3^{B}Fe(NNH_2)^+$, with respect to one-electron reduction.

We conclude that facile reduction of $P_3^{B}Fe(NNH_2)^+$ to $P_3^{B}Fe(NNH_2)$, relative to that for $P_3^{Si}Fe(NNH_2)^+$ and $P_3^{C}Fe(NNH_2)^+$, is one important factor in determining its comparative efficiency for N_2RR. As further elaborated below, long-lived $P_3^{E}Fe(NNH_2)^+$ intermediates can, via bimolecular PCET pathways, instead lead to unproductive HER. This HER activity, however, is dependent on both a long-lived $P_3^{E}Fe(NNH_2)^+$ intermediate, and the presence of a highly reactive PCET reagent, such as a $P_3^{E}Fe(NNH_2)$ species. We have previously postulated that $P_3^{E}Fe(NNH_2)$ formation is required for the release of the first equivalent of NH_3 and thus suggest that this species may be a crucial intermediate in both HER and N_2RR.[4fg,17]

Calculated PCET Reactions

The differences in N–H bond strengths and relative rates of $P_3^{E}Fe(NNH_2)^+$ reduction, with corresponding implications for product selectivity, are further highlighted by calculating the thermodynamic and kinetic parameters for several PCET reactions of interest (Figure 4ABC). In particular, comparative driving forces were calculated for unproductive bimolecular PCET reactions that generate H_2 between $P_3^{E}Fe(NNH_2)^{n+}$ (n = 0,1; E = B, Si, C) and $P_3^{E}Fe(NNH_2)$. Consistent with the calculated $BDFE_{N–H}$ values (Figure 3), the $P_3^{Si}Fe$, and to a lesser extent the $P_3^{C}Fe$, system shows a higher propensity to undergo PCET to liberate H_2 and the corresponding reduced Fe–NNH_y species. This is especially apparent in the reaction between two $P_3^{E}Fe(NNH_2)^+$ species, and in the cross-reaction between an $P_3^{E}Fe(NNH_2)^+$ cation and a neutral $P_3^{E}Fe(NNH_2)$ species.

In the former case, two $P_3^{E}Fe(NNH_2)^+$ (E = Si, C) species react in a very favorable step to form 0.5 equiv H_2 and $P_3^{E}Fe(NNH)^+$ (ΔG_{calc} = −17.5 kcal/mol and −16.5, respectively; Figure 4A). The reaction barrier is expected to be dominated in this case by the work required to bring two cationic species together in solution (~5 kcal/mol; see SI), highlighting the reactive nature of $P_3^{C/Si}Fe(NNH_2)^+$. In contrast, $P_3^{B}Fe(NNH_2)^+$ shows a correspondingly uphill PCET reaction (ΔG_{calc} = +3.1 kcal/mol) in its self-combination to liberate H_2 and $P_3^{B}Fe(NNH)^+$;[23] $P_3^{B}Fe(NNH_2)^+$ 2 is also much more readily reduced to $P_3^{B}Fe(NNH_2)$ (Table 1).

The bimolecular reaction between cationic $P_3^{E}Fe(NNH_2)^+$ with $P_3^{E}Fe(NNH_2)$ to produce H_2 and the corresponding $P_3^{E}Fe(NNH)^+$ and $P_3^{E}Fe(NNH)$ byproducts is predicted to be favorable for all three systems (Figure 4C). However, the $P_3^{C/Si}Fe$ systems proceed with far more driving force than the $P_3^{B}Fe$ system.

Favorable driving forces are also predicted for all three systems in self reactions of $P_3^{E}Fe(NNH_2)$ to produce H_2 and $P_3^{E}Fe(NNH)$, but again the $P_3^{C/Si}Fe$ systems proceed with far more driving force (Figure 4B). While the bimolecular reaction of $P_3^{E}Fe(NNH_2)$ with

itself is therefore a presumed source of H_2 for each system, in sum the $P_3^{C/Si}Fe$ systems are more likely, under each of the considered bimolecular reactions, to liberate H_2, in accord with their efficiency for HER versus N_2RR relative to the $P_3^{B}Fe$ system.

Given that the reduction of $P_3^{C/Si}Fe(NNH_2)^+$ is predicted to be comparatively slow, one might expect such a species to build-up as an intermediate. This possibility warrants future experimental studies aimed at in situ detection. At the present stage, we can suggest that a high (relative) concentration of $P_3^{C/Si}Fe(NNH_2)^+$, and a high predicted propensity for HER via reaction of this species with either itself or $P_3^{C/Si}Fe(NNH_2)$, leads to unproductive PCET steps that evolve H_2 as competitive with downstream N_2 reduction steps that lead to N_2RR. This is one important factor in determining selectivity.

Since the $P_3^{B}Fe(NNH_2)^+$ intermediate is predicted to have a lower propensity for H_2-liberating PCET reactivity, and is also predicted to be reduced much more rapidly, the reaction of two $P_3^{B}Fe(NNH_2)$ molecules is a more probable source of H_2 for this scaffold; the efficiency for N_2RR on $P_3^{B}Fe$ should therefore be related to the rate at which $P_3^{B}Fe(NNH_2)$ can be productively consumed (i.e., protonated to form a $P_3^{B}Fe(NHNH_2)^+$ or $P_3^{B}Fe(NNH_3)^+$). Mechanistic experiments to address these scenarios are ongoing. For example, a recent study has shown that $P_3^{B}Fe(NNH_2)$ can be protonated by strong acid at low temperature to liberate $P_3^{B}Fe(N)^+$ and NH_3, presumably via $P_3^{B}Fe(NNH_3)^+$.[17]

While the $P_3^{C}Fe$ scaffold provides a less definitive comparison, the calculated $BDFE_{N–H}$ values and H_2-evolving PCET thermodynamics suggest that the dominant source of HER on the $P_3^{C/Si}Fe$ scaffolds may be the reaction between $Fe(NNH_2)$ and $Fe(NNH_2)^+$. The highly reducing nature of $P_3^{C}Fe(NNH_2)^+$, as for the P_3^{Si} scaffold, suggests it should be comparatively long-lived, and thus more likely to undergo PCET with $P_3^{C}Fe(NNH_2)$. The similarity between $P_3^{C}Fe$ and $P_3^{Si}Fe$ in their thermodynamics for the reaction between two $Fe(NNH_2)^+$ species (Figure 4A) does not correlate with their disparate $\%NH_3$ efficiencies. Substantial differences in their predicted thermodynamics for the reaction between $Fe(NNH_2)$ and $Fe(NNH_2)^+$ (Figure 4C) are more in line with the observed trend. This type of bimolecular reactivity may be an important source of HER on the $P_3^{C/Si}Fe$ scaffolds (Figure 5).

Wiberg Bond Indices of $P_3^{E}Fe(NxHy)$ Species

We next examine how each P_3^{E} auxiliary, and the corresponding $P_3^{E}Fe(NNH_y)$ valence at iron, confers variability in bonding to, and the electronic structure of, the NNH_y ligand, as a means of further considering corresponding reactivity differences of $P_3^{E}Fe(NNH_y)$ species.

Wiberg bond indices provide a means to examine how the localized bonding between various atoms, expressed as a bond index,[24] changes as a function of the NNH_y reduction state (i.e., NNH to NNH_2). We have suggested elsewhere that the relative flexibility of the P_3^{B} ligand, owing to a weak and dative Fe→B interaction, may allow for stabilization of $Fe–NNH_y$ intermediates where Fe–N pi-bonding is accompanied by pyramidalization at the Fe center, and a corresponding lengthening of the Fe–B distance.[4a,17,25] The P_3^{Si} ligand is expected to give rise to a more shared, covalent Fe–Si interaction, irrespective of the NNH_y

reduction state, and the P_3^C system may be expected to fall in the middle of these extremes. [4b]

Changes in the respective bond indices of these frameworks have been determined between pairs of P_3^EFe(NNH) and P_3^EFe(NNH_2) species (E = B, C, Si), related by formal addition of an H-atom to the former. Interestingly, the N–H bond indices are essentially invariant across all complexes studied, indicating that differences in $BDFE_{N–H}$ are mostly dependent on the relative bonding through the E–Fe–N–N manifold. [26] The most salient data, reproduced in Figure 6, are the total Wiberg bond indices for Fe–N_α, Fe–N_β, Fe–E, N–N and N–H. The total Fe–N–N bond order, Σ(Fe–N–N), is also provided, as is the net difference in the $\Delta BDFE_{N\text{-}H}$ value, for each pair on moving from Fe(NNH) to Fe(NNH_2).

As expected, the Fe–E bond order weakens slightly from Fe(NNH) to Fe(NNH_2) for E = B, and stays constant for both Si and C. The respective change at Fe-N_α is also informative. For the B system, a significant increase is observed (1.6 to 1.9), reflecting a build-up in pi-bonding in P_3^BFe(NNH_2), akin to low-spin (pseudotetrahedral) iron imides of the type P_3^BFe(NR). For comparison, a previously characterized P_3^BFe(NR) species (R = 4-OMe-Ph) is predicted to have an Fe–N bond order of 1.8 (see SI).

By contrast, the Fe–N_α index for Si is sharply attenuated (from 1.6 to 1.2), reflecting a corresponding decrease in pi bonding. While this difference must partly reflect a less flexible Fe-Si interaction, it also reflects the electronic structure resulting from an extra electron in the frontier orbitals of the ^2E {Fe-Si}^{7} system relative to ^1A {Fe-B}^{6}. Interestingly, P_3^BFe(NNH_2) is pyramidalized at N_β whereas N_β is planar for P_3^{Si}Fe(NNH_2). This observation can again be rationalized by the assignment of a low-spin iron “imide-like” electronic structure to {Fe-B}^{6} P_3^BFe(NNH_2), but not for {Fe-Si}^{7} P_3^{Si}Fe(NNH_2), where substantial spin leaks onto the NNH_2 subunit (19% on P_3^{Si}Fe(NNH_2)). The C system provides an interesting further comparison, with spin leakage onto the NNH_2 unit falling between these two extremes (12% on P_3^CFe(NNH_2)). An increase in the Fe-N_α index occurs from P_3^CFe(NNH) to P_3^CFe(NNH_2) (1.2 to 1.4), but N_β is predicted to remain planar.

There also appears to be a strong trend between the degree of change in the total Fe–N–N bond order (Σ(Fe–N–N)) and the $\Delta BDFE_{N\text{-}H}$; The B and C systems show little change in Σ(Fe–N–N), with a corresponding significant increase in $BDFE_{N\text{-}H}$ from Fe(NNH) to Fe(NNH_2) (7.0 and 17.9 kcal/mol, respectively). However, the P_3^CFe system starts at a much weaker $BDFE_{N\text{-}H}$ of 17.3 kcal/mol for P_3^CFe(NNH) (compared to 31.2 kcal/mol for P_3^BFe). This observation is consistent with their total Σ(Fe–N–N) values (3.8 for B and 2.9 for C). Thus, the comparative stability of P_3^CFe(NNH_2), with its much higher $BDFE_{N\text{-}H}$ relative that in P_3^CFe(NNH), appears to reflect a higher degree of instability in P_3^CFe(NNH) (relative to the same comparison for E = B). This idea is further supported by Wiberg bond indices of the P_3^EFe(N_2) species, which show a total bond order of 4.0 across the Fe–N–N unit for all three scaffolds **(Figure 6)**.

In sharp contrast, the P_3^{Si}Fe system has a relatively high Σ(Fe–N–N) value in P_3^{Si}Fe(NNH), but this value decreases dramatically in P_3^{Si}Fe(NNH_2). There is correspondingly very little change in the $\Delta BDFE_{N\text{-}H}$, reflecting a comparatively very weak N-H bond in P_3^{Si}Fe(NNH_2).

The instability of $P_3^{Si}Fe(NNH_2)$, with an electronic structure that places substantial unpaired spin on NNH_2 owing to the $\{Fe\text{-}Si\}^7$ configuration, presumably contributes to the cathodically shifted reduction potential predicted for $P_3^{Si}Fe(NNH_2)^+$ relative to $P_3^{B}Fe(NNH_2)^+$, and also its propensity for facile PCET to liberate H_2.

The $P_3^{B}Fe$ system is unique within this series in its ability to support a high total Fe–N–N bond order from Fe(NNH) to $Fe(NNH_2)$, facilitating its trajectory along productive N_2RR.

Conclusion

Exploring the chemical basis for N_2RR versus HER selectivity for a molecular catalyst is important to future catalyst design. The DFT study described herein suggests that PCET reactions involving $P_3^{E}Fe(NNH_2)^{n+}$ species likely play an important role in the efficiency of N_2-to-NH_3 conversion catalysis by $P_3^{E}Fe$ model systems. These calculations enable predictions qualitatively consistent with previous stoichiometric and catalytic experiments. The comparative stability of $P_3^{E}Fe(NNH_2)^{n+}$ intermediates, as predicted by calibrated $BDFE_{N–H}$ values and redox potentials, emerges as one of the important factors in determining selectivity for N_2RR versus HER in these systems. Corresponding Wiberg bond indices intimate P_3^{B} as an especially well-equipped ligand for supporting N_2RR at Fe, due to its high degree of flexibility and the valence electron count it confers to Fe in the reduced intermediate $P_3^{B}Fe(NNH_2)$. Our study suggests that increasing the rate at which an $P_3^{E}Fe(NNH_2)$ intermediate is productively consumed so as to avoid bimolecular HER, possibly via rapid PCET reagents, may be a promising route to increasing efficiency for NH_3 production.

Looking beyond these iron model systems, our study underscores the potential utility of DFT-predicted $BDFE_{N\text{-}H}$ determinations towards the rational design of catalysts for N_2RR. Intermediates with weak N–H bonds (e.g., M(NNH) and $M(NNH_2)$) are highlighted as important sources of H_2 production via bimolecular PCET. Such a scenario is distinct from HER activity via more traditional metal-hydride intermediates.

Supplementary Material

Refer to Web version on PubMed Central for supplementary material.

ACKNOWLEDGMENT

This work was supported by the NIH (GM 070757) and the Gordon and Betty Moore Foundation, and the Extreme Science and Engineering Discovery Environment (XSEDE), which is supported by National Science Foundation grant number ACI-1053575. B.D.M. acknowledges the support of the NSF for a Graduate Fellowship (GRFP). We thank Matthew Chalkley for insightful input.

Funding Sources

No competing financial interests have been declared.

REFERENCE

1 (a). Chatt J, Dilworth JR, Richards RL. Chem. Rev. 1978; 78:589–625.(b) Schrock RR. Acc. Chem. Res. 2005; 38:955–962. [PubMed: 16359167] Nishibayashi Y. Inorg. Chem. 2015; 54:9234–

9247. [PubMed: 26131967] (d) van der Ham CJM, Koper MTM, Hetterscheid DGH. Chem. Soc. Rev. 2014; 43:5183–5191. [PubMed: 24802308] (e) Shaver MP, Fryzuk MD. Adv. Synth. Catal. 2003; 345:1061–1076.(f) MacLeod KC, Holland PL. Nat. Chem. 2013; 5:559–565. [PubMed: 23787744]

2 (a). Howard JB, Rees DC. Proc. Nat. Acad. Sci. 2006; 103:17088–17093. [PubMed: 17088547] (b) Howard JB, Rees DC. Chem. Rev. 1996; 96:2965–2982. [PubMed: 11848848]

3. Hoffman BM, Lukoyanov D, Yang Z-Y, Dean DR, Seefeldt LC. Chem. Rev. 2014; 114:4041–4062. [PubMed: 24467365]

4 (a). Anderson JS, Rittle J, Peters JC. Nature. 2013; 501:84–87. [PubMed: 24005414] (b) Creutz SE, Peters JC. J. Am. Chem. Soc. 2014; 136:1105–1115. [PubMed: 24350667] (c) Ung G, Peters JC. Angew. Chem., Int. Ed. 2015; 54:532–535.(d) Del Castillo TJ, Thompson NB, Peters JC. J. Am. Chem. Soc. 2016; 138:5341–5350. [PubMed: 27026402] (e) Chalkley MJ, Del Castillo TJ, Matson BD, Roddy JP, Peters JC. ACS Central Science. 2017; 3:217–223. [PubMed: 28386599] (f) Anderson JS, Cutsail GE, Rittle J, Connor BA, Gunderson WA, Zhang L, Hoffman BM, Peters JC. J. Am. Chem. Soc. 2015; 137:7803–7809. [PubMed: 26000443] (g) Rittle J, Peters JC. J. Am. Chem. Soc. 2016; 138:4243–4248. [PubMed: 26937584] (h) Rittle J, Peters JC. J. Am. Chem. Soc. 2017; 139:3161–3170. [PubMed: 28140600]

5 (a). Kuriyama S, Arashiba K, Nakajima K, Matsuo Y, Tanaka H, Ishii K, Yoshizawa K, Nishibayashi Y. Nat. Commun. 2016; 7:12181. [PubMed: 27435503] (b) Yandulov DV, Schrock RR. Science. 2003; 301:76–78. [PubMed: 12843387] (c) Arashiba K, Miyake Y, Nishibayashi Y. Nat. Chem. 2011; 3:120–125. [PubMed: 21258384] (d) Kuriyama S, Arashiba K, Nakajima K, Tanaka H, Kamaru N, Yoshizawa K, Nishibayashi Y. J. Am. Chem. Soc. 2014; 136:9719–9731. [PubMed: 24896850] (e) Arashiba K, Kinoshita E, Kuriyama S, Eizawa A, Nakajima K, Tanaka H, Yoshizawa K, Nishibayashi Y. J. Am. Chem. Soc. 2015; 137:5666–5669. [PubMed: 25879994]

6 (a). Del Castillo TJ, Thompson NB, Suess DLM, Ung G, Peters JC. Inorg. Chem. 2015; 54:9256–9262. [PubMed: 26001022] (b) Kuriyama S, Arashiba K, Tanaka H, Y. Matsuo Y, Nakajima K, Yoshizawa K, Nishibayashi Y. Angew. Chem. Int. Ed. 2016; 55:14291–14295.

7 (a). Reiher M, Le Guennic B, Kirchner B. Inorg. Chem. 2005; 44:9640–9642. [PubMed: 16363831] (c) Studt F, Tuczek F. Angew. Chem. Int. Ed. 2005; 44:5639–5642.(d) Studt F, Tuczek F. J. Comput. Chem. 2006; 27:1278–1291. [PubMed: 16786542] (e) Ujjal Gogoi U, Kanti Guha A, Phukan AK. Chem. Eur. J. 2013; 19:11077–11089. [PubMed: 23821310]

8. Side-by-side comparisons of catalytic N_2RR by P_3^EFe (E = B, C, and Si) using potassium graphite (KC_8) and $[(Et_2O)_2H][BAr^F{}_4]$ ($HBAr^F{}_4$, $BAr^F{}_4$ = tetrakis-(3,5-bis(trifluoromethyl)phenyl)borate) have revealed P_3^BFe to be the most efficient catalyst, with reported efficiencies up to 37%. N_2RR catalysis by P_3^CFe or $P_3^{Si}Fe$ is less efficient under these conditions, with reported efficiencies of 33% and 4%, respectively. Studies focused on HER catalysis have shown $P_3^{Si}Fe(N_2)^-$ (88% per H^+) to be significantly more efficient than $P_3^BFe(N_2)^-$ (40% per H^+) under analogous conditions. See 4d.

9 (a). Warren JJ, Tronic TA, Mayer JM. Chem. Rev. 2010; 110:6961–7001. [PubMed: 20925411] (b) Hammes-Schiffer S. J. Am. Chem. Soc. 2015; 137:8860–8871. [PubMed: 26110700]

10. Grimme S, Antony J, Ehrlich S, Krieg H. J. Chem. Phys. 2010; 132:154104. [PubMed: 20423165]

11. Tao JM, Perdew JP, Staroverov VN, Scuseria GE. Phys. Rev. Lett. 2003; 91:146401. [PubMed: 14611541]

12. Weigend F, Ahlrichs R. Phys. Chem. Chem. Phys. 2005; 7:3297–3305. [PubMed: 16240044]

13. Valiev M, Bylaska EJ, Govind N, Kowalski K, Straatsma TP, Van Dam HJJ, Wang D, Nieplocha J, Apra E, Windus TL, de Jong WA. Comput. Phys. Commun. 2010; 181:1477–1489.

14. Neese F. Wiley Interdiscip. Rev. Comput. Mol. Sci. 2012; 2:73–78.

15 (a). Klamt A, Schüürmann G. J. Chem. Soc. Perkin Trans. 2. 1993; 2:799–805.(b) Marten B, Kim K, Cortis C, Friesner RA, Murphy RB, Ringnalda MN, Sitkoff D, Honig B. J. Phys. Chem. 1996; 100:11775–11788.

16 (a). Ribeiro RF, Marenich AV, Cramer CJ, Truhlar DG. J. Phys. Chem. B. 2011; 115:14556–14562. [PubMed: 21875126] (b) Wang T, Brudvig G, Batista VS. J. Chem. Theory Comput. 2010; 6:755–760. [PubMed: 20607115] (c) Marten B, Kim K, Cortis C, Friesner RA, Murphy RB, Ringnalda MN, Sitkoff D, Honig B. J. Phys. Chem. 1996; 100:11775–11788.

17. Thompson NB, Green MT, Peters JC. J. Am. Chem. Soc. 2017; 139:16105–16108. [PubMed: 29073760]

18. Marcus RA. J. Chem. Phys. 1956; 24:966–978.

19 (a). Dempsey JL, Brunschwig BS, Winkler JR, Gray HB. Acc. Chem. Res. 2009; 42:1995–2004. [PubMed: 19928840] (b) Lewandowska-Andralojc A, Baine T, Zhao X, Muckerman JT, Fujita E, Polyansky DE. Inorg. Chem. 2015; 54:4310–4321. [PubMed: 25902004] (c) Yang JY, Smith SE, Liu T, Dougherty WG, Hoffert WA, Kassel WS, DuBois MR, DuBois DL, Bullock RM. J. Am. Chem. Soc. 2013; 135:9700–9712. [PubMed: 23631473]

20. Brookhart M, Grant B, Volpe AF Jr.. Organometallics. 1992; 11:3920–3922.

21. Fajardo J, Peters JC. J. Am. Chem. Soc. 2017; 139:16105–16108. [PubMed: 29073760]

22. We have previously reported bond dissociation enthalpies ($BDE_{N\text{-}H}$) for $P_3^BFe(NNH)$ and $P_3^BFe(NNH_2)$ (see ref 4e). Here we reported $BDFE_{N\text{-}H}$ values as they have more theoretical justification in the absence of experimental knowledge of the entropy change associated with H· loss.

23. While this discussion may seem at odds with the enhanced stability of $P_3^{Si}Fe(NNH_2)^+$ relative to $P_3^BFe(NNH_2)^+$, other factors are presumably responsible in solution, such as the more facile reduction of $P_3^BFe(NNH_2)^+$ relative to $P_3^{Si}Fe(NNH_2)^+$.

24. Wiberg KB. Tetrahedron. 1968; 24:1083–1096.

25. Moret M-E, Peters JC. J. Am. Chem. Soc. 2011; 133:18118–18121. [PubMed: 22008018]

26. Similarly, the C_2H_5 radical is predicted to have a very low $BDFE_{C\text{-}H}$ (34 kcal/mol) when compared to C_2H_4 (100 kcal/mol), but the Wiberg bond indices for their respective C–H bonds do not change appreciably (See SI).

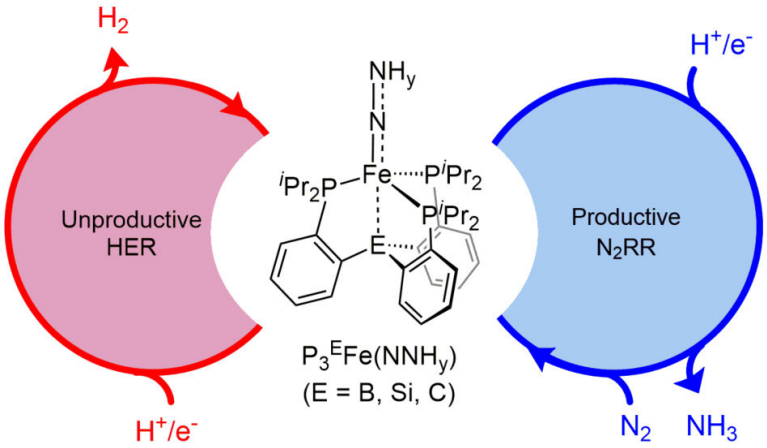

Figure 1.

Schematic depiction of N_2RR/HER iron catalysts studied herein to explore key factors dictating product selectivity.

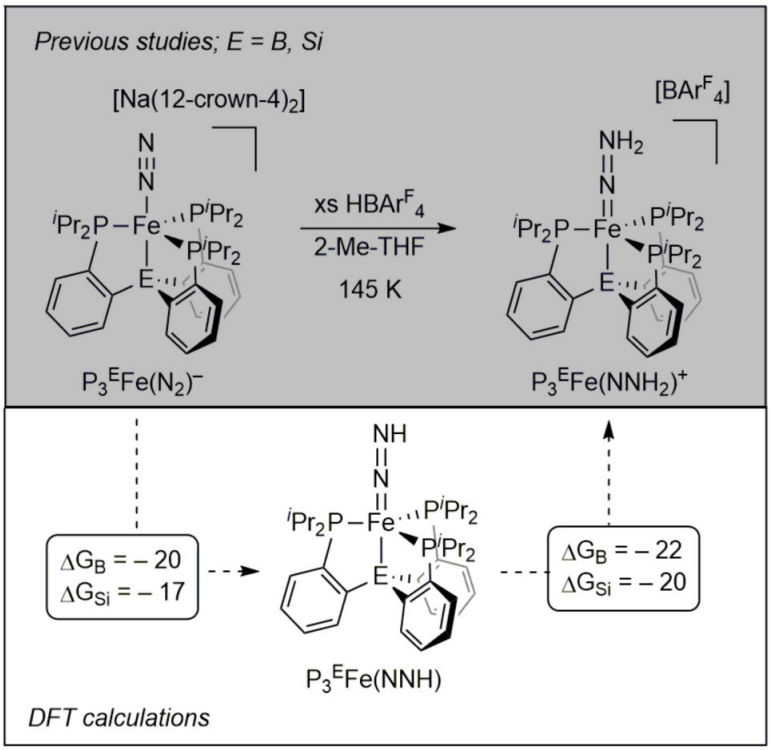

Figure 2.

(top) Previous experimental work showing the formation of $P_3^EFe(NNH_2)^+$ (E = B or Si) via protonation with excess acid.[4f,g] (bottom) Calculated free energy changes (in kcal/mol; 195 K) for the formation of $P_3^EFe(NNH_2)^+$ via $P_3^EFe(NNH)$ (E = B or Si).

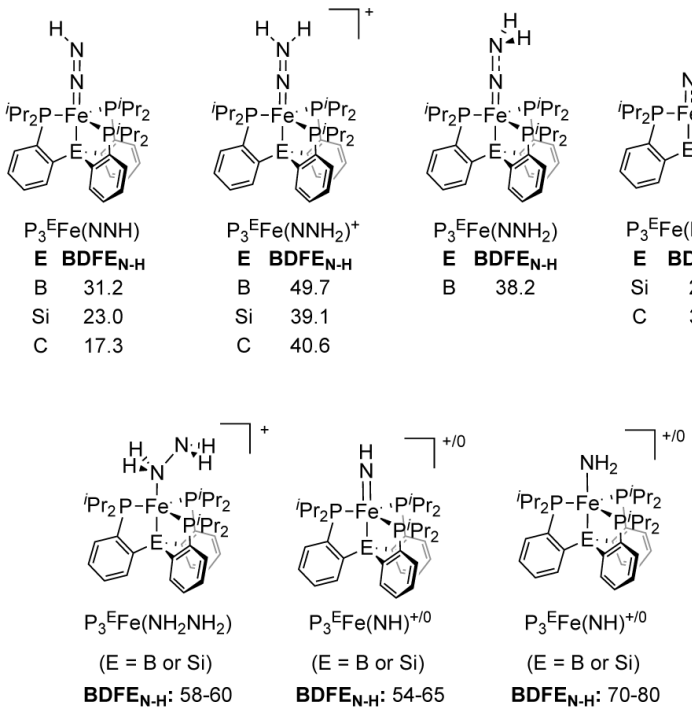

Figure 3.
$BDFE_{N–H}$ values (in kcal/mol) for selected $P_3^EFe(N_xH_y)$ species.[22]

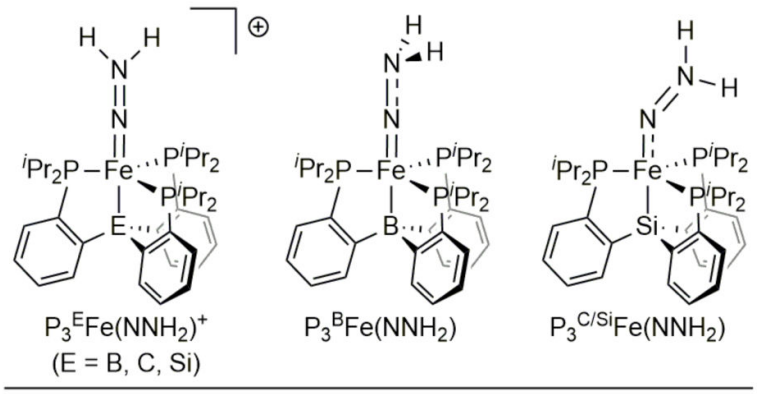

			ΔG$_{calc}$		
			E = B	E = C	E = Si
A	$P_3^EFe(NNH_2)^+$ + $P_3^EFe(NNH_2)^+$	$-H_2$ → $P_3^EFe(NNH)^+$ + $P_3^EFe(NNH)^+$	+3.1	-16.5	-17.5
B	$P_3^EFe(NNH_2)$ + $P_3^EFe(NNH_2)$	$-H_2$ → $P_3^EFe(NNH)$ + $P_3^EFe(NNH)$	-22.7	-34.3	-54.9
C	$P_3^EFe(NNH_2)^+$ + $P_3^EFe(NNH_2)$	$-H_2$ → $P_3^EFe(NNH)^+$ + $P_3^EFe(NNH)$	-9.8	-25.4	-36.0

Figure 4.

Calculated free energy changes (ΔG_{calc}; in kcal/mol; 195 K) for several putative PCET reactions that evolve H_2.

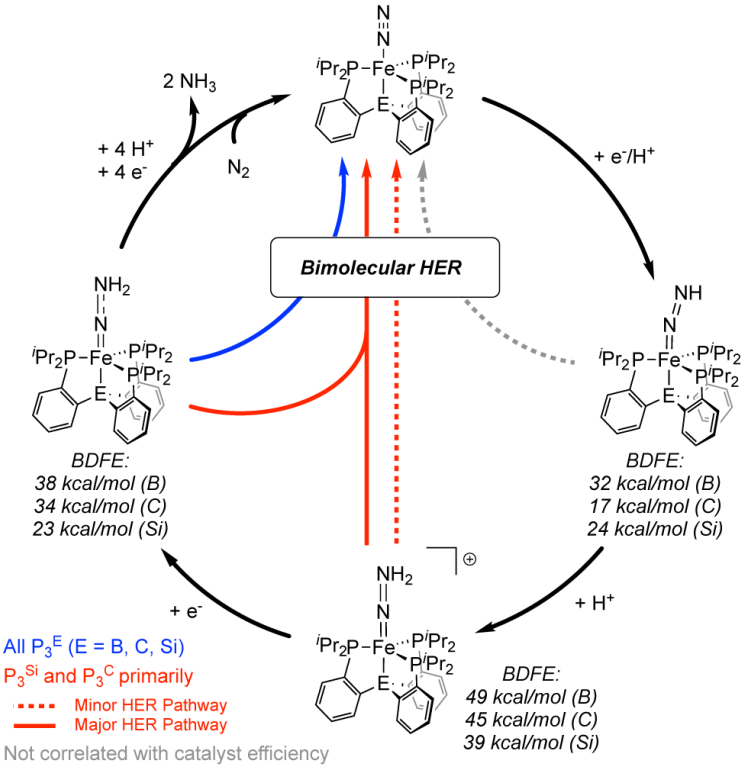

Figure 5.

Overview of predicted bimolecular HER and N_2RR pathways for $P_3^EFe(NNH_y)$ species and pertinent $BDFE_{N–H}$ values.

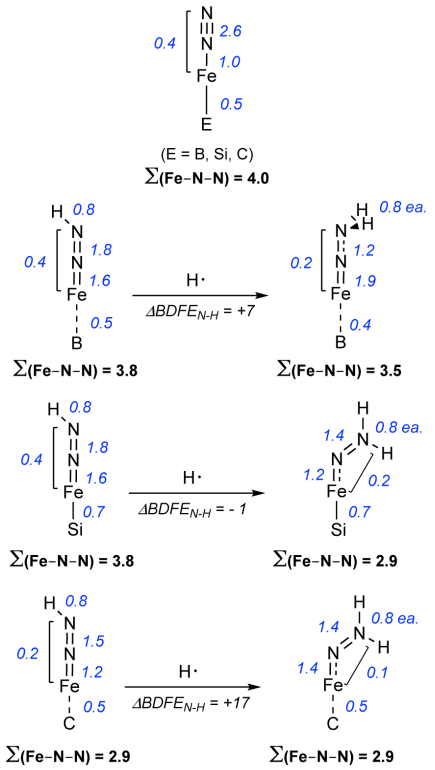

Figure 6.

Selected total Wiberg bond indices for $P_3^EFe(N_2)$, $P_3^EFe(NNH)$ and $P_3^EFe(NNH_2)$ species, along with the total Fe–N–N bond order, Σ(Fe–N–N). $\Delta BDFE_{N\text{-}H}$ values are reported in kcal/mol.

Table 1

Calculated thermodynamic and kinetic parameters for $P_3^EFe(NNH_2)^+ \rightarrow P_3^EFe(NNH_2)$[a]

	$P_3^EFe(NNH_2)^+ + e^- \rightarrow P_3^EFe(NNH_2)$			
	E° (vs $Fc^{+/0}$)	**$\lambda_{is,ET}$**	**G^*_{rel}[b]**	**k_{rel}[b]**
E = B	−1.2 V	23	1.0	1
E = Si	−1.9 V	30	4.4	2×10^{-4}
E = C	−2.0 V	30	5.2	2×10^{-5}

[a] Energies are in kcal/mol, unless noted otherwise.

[b] G^*_{rel} values were calculated assuming a $P_3^BFe(NNH_2)^+$ reduction barrier of 1.0 kcal/mol. $k_{rel} \equiv \exp[(G^*_B - G^*_E)/k_bT]$ where T = 195 K.M